Science Bulletin 66 (2021) 339–346

Contents lists available at ScienceDirect

Science Bulletin

journal homepage: www.elsevier.com/locate/scib

Article

Efficient and stable inverted perovskite solar cells enabled by inhibition of self-aggregation of fullerene electron-transporting compounds

Chengbo Tian [a,*], German Betancourt-Solis [b], Ziang Nan [c], Kaikai Liu [a], Kebin Lin [a], Jianxun Lu [a], Liqiang Xie [a], Luis Echegoyen [b,*], Zhanhua Wei [a,*]

[a] Institute of Luminescent Materials and Information Displays, College of Materials Science and Engineering, Huaqiao University, Xiamen 361021, China
[b] Department of Chemistry, University of Texas at El Paso, El Paso, TX 79968, USA
[c] iChEM (Collaborative Innovation Center of Chemistry for Energy Materials), Department of Chemistry, College of Chemistry and Chemical Engineering, Xiamen University, Xiamen 361005, China

ARTICLE INFO

Article history:
Received 20 June 2020
Received in revised form 11 July 2020
Accepted 31 July 2020
Available online 01 September 2020

Keywords:
Functionalized fullerene
Self-aggregation
Intermolecular interaction
Operation stability
Inverted perovskite solar cells

ABSTRACT

Fullerene-based electron-transporting layers (ETLs) significantly influence the defect passivation and device performance of inverted perovskite solar cells (PSCs). However, the π-cage structures of fullerenes lead to a strong tendency to self-aggregate, which affects the long-term stability of the corresponding PSCs. Experimental results revealed that [6,6]-phenyl-C_{61}-butyric acid methyl ester (PCBM)-based ETLs exhibit a certain degree of self-aggregation that affects the stability of the device, particularly under continuous irradiation stress. To modulate the aggregation behavior, we replaced a methyl hydrogen of PCBM with a phenyl group to yield [6,6]-phenyl-C_{61}-butyric acid benzyl ester (PCBB). As verified through X-ray crystallography, this minor structural modification results in more non-covalent intermolecular interactions, which effectively enhanced the electron-transporting ability of the PCBB-based ETL and led to an efficiency approaching 20%. Notably, the enhanced intermolecular forces of PCBB suppressed its self-aggregation, and the corresponding device showed significantly improved stability, retaining approximately 90% of its initial efficiency after 600 h under one-sun irradiation with maximum power point tracking. These findings provide a viable approach for the design of new fullerene derivatives to tune their intermolecular interactions to suppress self-aggregation within the ETL for high-performance PSCs.

1. Introduction

Organic and inorganic lead halide perovskites are excellent photovoltaic materials owing to their exceptional physical and chemical properties [1–7]. As a result of extensive research efforts to understand the underlying working mechanisms, the development of new materials, and the progress made in interface optimization [8–10], the power conversion efficiency (PCE) of a single-junction perovskite solar cell (PSC) has soared to over 25% in the past decade [11], which is comparable with the value for single-crystal silicon solar cells. Fullerene compounds are widely used as electron-transporting layers (ETLs) in inverted planar PSCs, and they have received considerable attention because of their simple device architecture, hysteresis-free performance, scalable preparation processes, and compatibility with flexible substrates and tandem photovoltaic devices [12–16].

In 2013, [6,6]-phenyl-C_{61}-butyric acid methyl ester (PCBM) was first introduced as an ETL into an inverted PSC architecture, and the unique features of fullerenes, such as high electron affinity, high electron mobility, and well-matched energy levels with the perovskites, were successfully verified [17]. Thereafter, Huang and co-workers [18] demonstrated that fullerene derivatives can not only serve as ETLs but also contribute by passivating the trap states at the surfaces and grain boundaries of perovskite layers, which can efficiently suppress the undesirable hysteresis and increase the PCE of the PSCs. A series of fullerene derivatives functionalized with cross-linkable groups [19], ester [20–23], amino [24–26], and pyridine groups [27,28] were designed and used in inverted PSCs as ETLs to enhance the electron extraction and passivation of fullerene/perovskite interface defects to achieve high efficiencies [29,30]. The PCEs of inverted devices have been greatly improved by tuning the interface through the optimization of the composition of the perovskite layers and using novel fullerene derivatives [31–34].

* Corresponding authors.
E-mail addresses: cbtian@hqu.edu.cn (C. Tian), echegoyen@utep.edu (L. Echegoyen), weizhanhua@hqu.edu.cn (Z. Wei).

https://doi.org/10.1016/j.scib.2020.08.041
2095-9273/

The role of fullerene compounds in device stability remains unclear. Although the stability of inverted PSCs has been greatly improved by modifying interfaces and using stable inorganic hole-transporting materials [35–37], fullerene-based ETLs must be thoroughly investigated to further extend the lifetimes of the PSCs. The self-aggregation behavior of fullerenes is believed to affect the long-term stability of inverted PSCs [38]; therefore, this process should be inhibited. Adding aromatic functional groups such as phenyl to fullerene derivatives enhances their intermolecular interactions [39,40], leading to the suppression of self-aggregation and resulting in more stable films that would improve the stability of inverted PSCs.

In this study, we found that the commonly used PCBM layer exhibited self-aggregation behavior under continuous irradiation, which resulted in reduced device stabilities and loss of performance. To further understand and control the influence of the molecular structure of the functionalized fullerene on the aggregation behavior, [6,6]-phenyl-C_{61}-butyric acid benzyl ester (PCBB) with one extra phenyl group was synthesized and incorporated into inverted PSCs as an ETL. Crystal structural analyses revealed that PCBB showed significantly enhanced intermolecular interactions, including π-π interactions between the C_{60} cages and CH-π interactions between functional groups, as compared with PCBM. These interactions could suppress aggregation within the fullerene-based ETLs. As a result, a champion device with PCBB as an ETL yielded a PCE of 19.84%. PCBB-based devices showed excellent long-term stability at the maximum power point (MPP) aging for 600 h, which was much better than that for PCBM-based devices. This work indicates that the inverted device performance, particularly long-term stability, can be improved by rationally designing fullerene derivatives to suppress self-aggregation in the films.

2. Materials and methods

2.1. Materials

PCBM was purchased from Nano-C, and PCBB was synthesized following Ref. [41]. The synthesis steps and characterization for other related materials are provided in the Supplementary materials. The other chemical reagents and materials for perovskite precursor solution such as formamidinium iodide (FAI), methylammonium iodide (MAI), PbI_2, $PbBr_2$, CsI, N,N-dimethylformamide (DMF), N-methyl-2-pyrrolidinone (NMP), and dimethyl sulfoxide (DMSO) were purchased from Sigma–Aldrich or Alfa-Aesar and used as received.

2.2. Device fabrication

The inverted PSCs with a configuration of FTO/NiO_x (nickel oxide)/perovskite/PCBM (or PCBB)/BCP/Ag were fabricated on the patterned FTO glass substrates with a resistivity of 7 Ω/cm^2. The patterned FTO glass substrates were sequentially cleaned with detergent, deionized water, acetone, and ethanol and then treated in a UV ozone oven for 30 min. The nickel oxide (NiO_x) precursor (0.6 mol/L) was prepared by dissolving nickel(II) nitratehexahydrate ($Ni(NO_3)_2{\cdot}6H_2O$) ethylene glycol with ethylenediamine and kept at 70 °C for 3 h in a sealed vial to form the NiO_x precursor solution as Ref. [38]. The NiO_x precursor solution was spin-coated on the FTO at 4000 r/min for 60 s in the glove box and annealed at 300 °C for 1 h in a muffle furnace. Then, 60 μL of triple-cation perovskite precursor solution was spin-coated at 1000 r/min for 10 s and 5000 r/min for 20 s (the perovskite precursor solution was prepared by dissolving FAI (353.2 mg), MAI (66.2 mg), CsI (33.8 mg), PbI_2 (1018.8 mg), and $PbBr_2$ (143.2 mg) in 2 mL of mixed anhydrous solvent of DMF/DMSO/NMP (with ratio of 40/9/1 by volume). And 200 μL of anhydrous chlorobenzene was dropped onto the substrates at 5 s before the end of the procedure. The as-prepared films were immediately annealed at 100 °C for 30 min. After cooling to room temperature, 2 wt% PCBM (or PCBB) dissolved in chlorobenzene was spin-coated on top of the perovskite layers. The BCP solution with a concentration of 0.5 mg/mL in 2-propanol was spin-coated on top of the fullerene layer at 5000 r/min for 30 s and annealed at 80 °C for 10 min. Silver electrodes (100 nm) were deposited by thermal evaporation under 1.0×10^{-4} Pa through a shadow mask to complete the devices.

2.3. Characterization

MALDI-time-of-flight (TOF) mass spectrometric measurements were conducted on a Bruker Microflex LRF mass spectrometer. The NMR spectra were recorded using a JEOL 600 MHz spectrometer. The UV/Vis spectra were obtained using a Cary 5000 spectrophotometer. Cyclic voltammetry (CV) experiments were carried out under an argon atmosphere at room temperature by using a CH Instrument Potentiostat. The scan rate for CV experiments was 100 mV/s. The diffraction data of single-crystal PCBB were tested on a Bruker SMART APEX CCD system equipped with a graphite monochromator and a Cu Kα fine-focus tube (λ = 1.54 184 Å). The contact angles of water droplets were determined by using a Ramé–Hart goniometer with pure deionized water at room temperature. Ten static measurements were analyzed and averaged for each film. The steady photoluminescence (PL) spectra were recorded using a F7000 Fluorescence Spectrophotometer (HITACHI). The time-resolved photoluminescence (TRPL) spectra were obtained on an Edinburgh instruments FLS980 fluorescence spectrometer. *J-V* curves of the PSCs were recorded using a Keithley 2420 source measure unit under a Photo Emission Tech SS100 Solar Simulator, and light intensity was calibrated with a standard Si solar cell. The external quantum efficiency (EQE) was determined on a Bentham (from Bentham Instruments Ltd.) measurement system in DC mode. Scanning electron microscopy (SEM) images were collected from a field emission scanning electron microscope (HITACHI S-4800), where the electron beam was accelerated in the range of 500 V to 20 kV.

3. Results and discussion

As shown in Scheme S1 (online), PCBB was synthesized following a previously reported synthetic method [41]. The chemical structures of the compounds were characterized by TOF mass spectrometry, ^{1}H and ^{13}C NMR (Figs. S1–S7 online). The molecular structure of PCBB was determined using X-ray single-crystal diffraction analysis. The PCBB crystals were grown by diffusing methanol into toluene solution at room temperature. As shown in Fig. 1a, the packing mode of PCBB molecules was viewed along the *a*-axis. More than three π-π interactions were noted between adjacent fullerene cages. The distance between π-π stacked groups was 3.20 Å, which was similar to inter C_{60}–C_{60} cage contacts for the most commonly used PCBM [42]. Compared with the intermolecular interactions observed within the PCBM crystal (refcode: EKOZUZ) (Fig. 1c), more π-π interactions were observed between the PCBB molecules. As shown in Fig. 1b and d, the functional group of PCBB interacted with eight nearby molecules through weak intermolecular interactions, while the functional group of PCBM only interacted with six nearby molecules. Therefore, the strong and numerous intermolecular interactions of PCBBs could increase the energy barrier of their molecular motion, thereby inhibiting aggregation behavior.

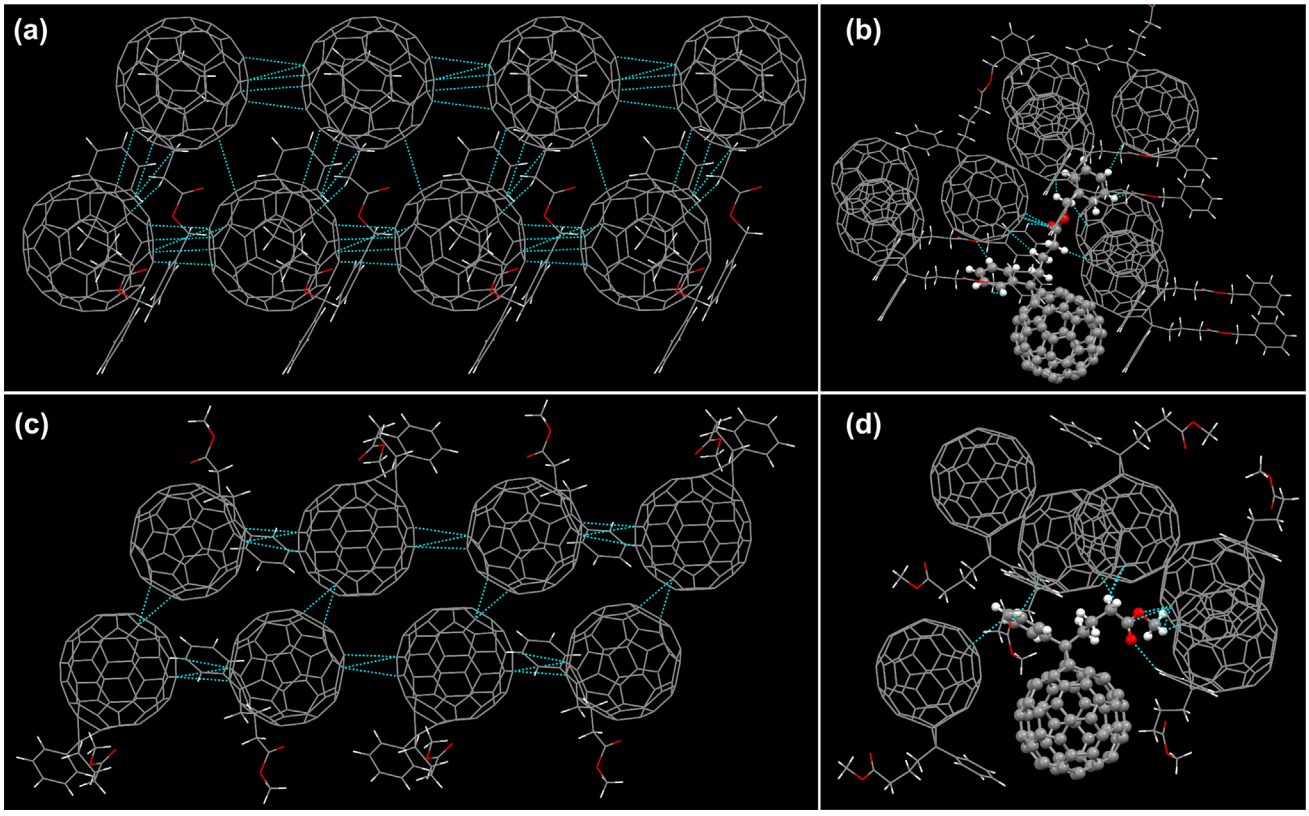

Fig. 1. Crystal packing and intermolecular interactions of (a, b) PCBB and (c, d) PCBM molecules. Gray: carbon; white: hydrogen; red: oxygen. The green dash line indicates the interaction between molecules.

As depicted in Fig. 2a, we proposed that the intermolecular interactions of the functionalized fullerene compounds could affect carrier transport and the stability of the corresponding ETLs. PCBB showed enhanced intermolecular interactions through π-π and CH–π interactions between the C_{60} cages and the functional groups, including the phenyl group. We assumed that these additional intermolecular interactions could inhibit fullerene aggregation in the films, leading to a highly stable film and high device stability. These intermolecular interactions should also lead to enhanced electron hopping between adjacent C_{60} cages and improved carrier collection efficiency [39,40]. Therefore, adding aromatic groups to the functionalized fullerene compounds was expected to suppress fullerene self-aggregation and increase the stability of the inverted PSCs. Meanwhile, electron transport in fullerene films depends on the delocalized π-π electron systems of the cages [43]. Combined with the abovementioned intermolecular interactions, PCBB-based films should exhibit higher electron mobility and more efficient carrier transport than PCBM-based films. To better understand the effect of molecular packing on charge transport, the space-charge limited current method and the Mott–Gurney law were employed to determine the electron mobilities of PCBB and PCBM (Fig. 2b) [44]. The electron-only devices with the configuration ITO/Cs_2CO_3/fullerene derivative/Ca/Al were prepared, and the mobilities of PCBM and PCBB were estimated to be 2.13×10^{-4} and 3.09×10^{-4} cm^2 V^{-1} s^{-1}, respectively. The high electron mobility for PCBB films could reasonably be attributed to compact molecular packing due to the enhanced intermolecular forces. The higher electron mobility of PCBB over PCBM facilitated electron transport in the inverted PSCs, thereby improving device performance.

The lowest unoccupied molecular orbital (LUMO) energy levels of PCBB and PCBM were investigated by CV (Fig. 2c). The LUMO energy levels of the fullerene derivatives were estimated from the onset reduction potentials (E_{red}^{on}) by using a previously reported equation [45]. The half-wave potentials and LUMO energy levels of the corresponding compounds are listed in Table S1 (online). The calculated LUMO level of PCBB was −3.90 eV, which was almost the same as that of PCBM (−3.91 eV). The suitable LUMO level of PCBB is critical for efficient inverted PSCs [22]. Combined with the optical bandgap of the fullerene derivatives evaluated through UV–vis absorption measurements (Fig. S8 and Table S1 online), the highest occupied molecular orbital energy levels of PCBB and PCBM were −5.62 and −5.64 eV, respectively, indicating good hole-blocking properties. As shown in Fig. 2d, the energy levels of PCBB matched well with those of the perovskite materials. The suitable energy level alignment should result in effective electron extraction at the perovskite/PCBB interface.

To evaluate PCBB-based ETLs, we fabricated inverted PSCs by using NiO_x and fullerene derivatives as the hole and electron extraction layers, respectively. The configuration and cross-sectional SEM images of the PSCs are shown in Fig. 3a and Fig. S9 (online), respectively. The thickness effect of PCBB-based ETLs on device performance was investigated by tuning the spin-coating speed for PCBB layer deposition. As shown in Fig. S10 and Table S2 (online), the highest device efficiency was obtained for a spin-coating speed of 3000 r/min, corresponding to a thickness of 60 nm. This speed was used to prepare all the devices. As shown in Fig. 3b, PSCs with PCBM and PCBB as ETLs showed different photovoltaic performance. The best PCBB-based cell yielded an overall PCE of 19.84% with V_{OC} of 1.08 V, J_{SC} of 22.85 mA/cm^2, and fill factor (FF) of 80.39%. By contrast, the best PCBM-based cell exhibited an inferior PCE of 18.30% due to a low V_{OC} of 1.06 V, J_{SC} of 22.53 mA/cm^2, and FF of 76.59% (reverse scan). The hysteresis effect of the devices was also studied by analyzing their *J-V* curves under

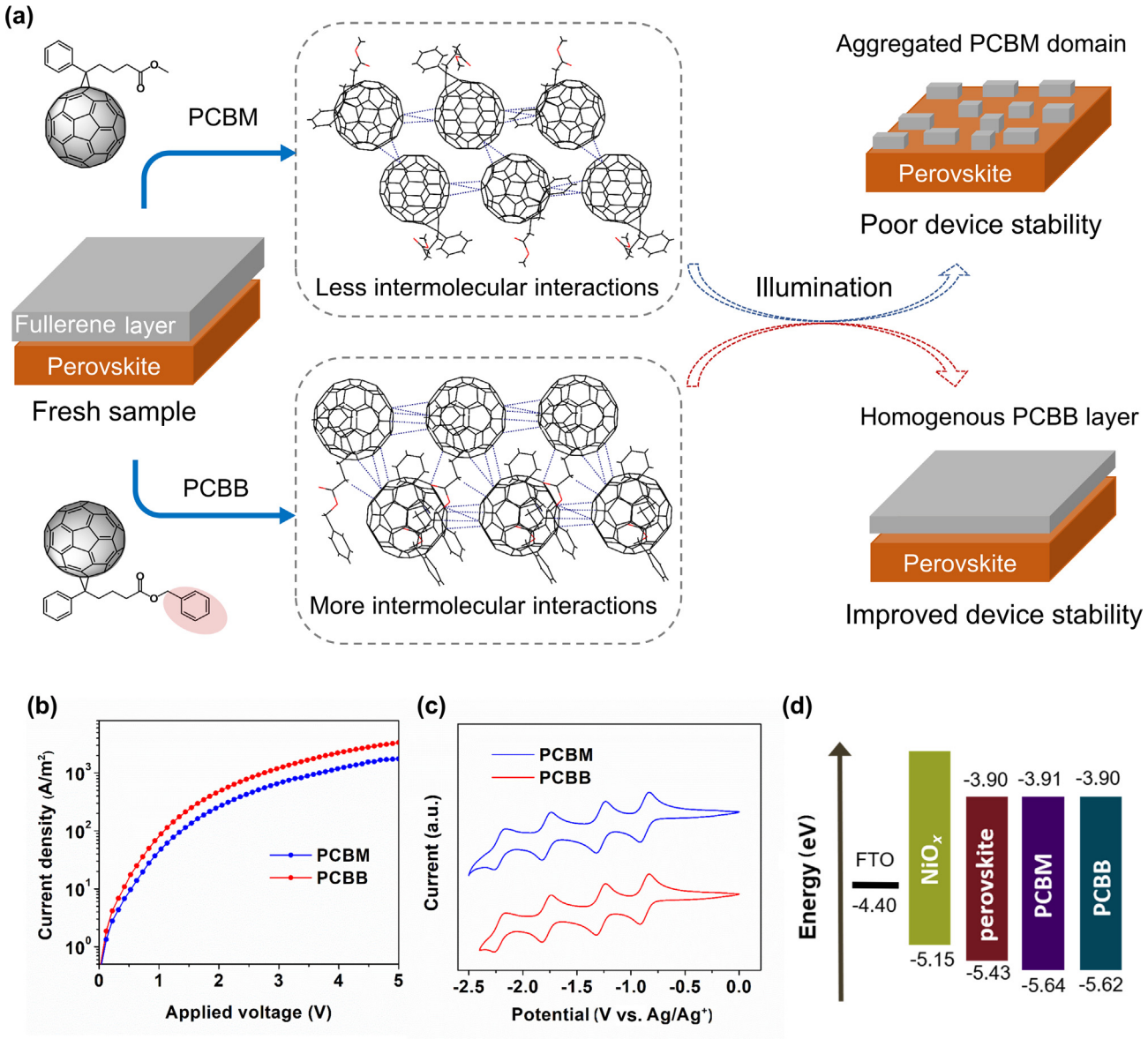

Fig. 2. Influence of fullerene's molecular structure and the characterization of fullerene material. (a) Schematic illustration of the influence of fullerene's intermolecular interaction on device stability. (b) Measured space-charge limited *J-V* curves of electron-only devices based on PCBM and PCBB. (c) Cyclic voltammetric curves for PCBM and PCBB at a scan rate of 100 mV/s. (d) Energy level diagram of the materials used in PSCs.

different scanning directions. As shown in Fig. S11 and Table S3 (online), PCBB-based devices showed slightly lower hysteresis than PCBM-based devices. The negligible hysteresis of PCBB-based cells could be attributed to efficient electron extraction at the fullerene/perovskite interface. We also assessed the incident photon-to-electron conversion efficiency (IPCE) spectrum to verify J_{SC} of the cells (Fig. 3c). Photocurrent densities of the PCBB- and PCBM-based devices were integrated from their corresponding IPCE curves and yielded values of 22.10 and 21.57 mA/cm^2, respectively. These values were in good agreement with the J_{SC} value described from the *J-V* curves.

The photovoltaic performance statistics of 60 individual cells (30 PCBB-based devices and 30 PCBM-based devices) are shown in Fig. 3d and Fig. S12 (online). The narrower PCE distribution of PCBB-based devices as compared with that of PCBM indicated excellent reproducibility. To further verify device performance, we tested the steady-state power output (SPO) of the PCBM-and PCBB-based devices for 200 s at their corresponding MPP determined from their *J-V* curves (Fig. 3e and f). PCBB-based devices yielded a steady-state PCE of 19.7% and a photocurrent density of 21.0 mA/cm^2 at 0.94 V, while PCBM-based devices showed a steady-state PCE of 18.1% and a photocurrent density of 20.6 mA/cm^2 at 0.88 V. Both SPOs of the PCBB- and PCBM-based cells were consistent with the values obtained from their corresponding *J-V* scans.

We conducted additional characterization to further understand why the use of PCBB as the ETL improved device efficiencies. To investigate the electron extraction ability of fullerenes, we performed steady-state PL and TRPL experiments. Samples of glass/perovskite, glass/perovskite/PCBM, and glass/perovskite/PCBB were prepared. As shown in Fig. 3g, all the samples exhibited a PL peak near 777 nm under 450-nm excitation. The PCBM- and PCBB-based ETLs showed obvious PL quenching, indicating effective electron extraction of the fullerene ETLs. Compared with PCBM-coated perovskite films, PCBB-coated perovskite films displayed slightly lower PL intensity, implying efficient electron

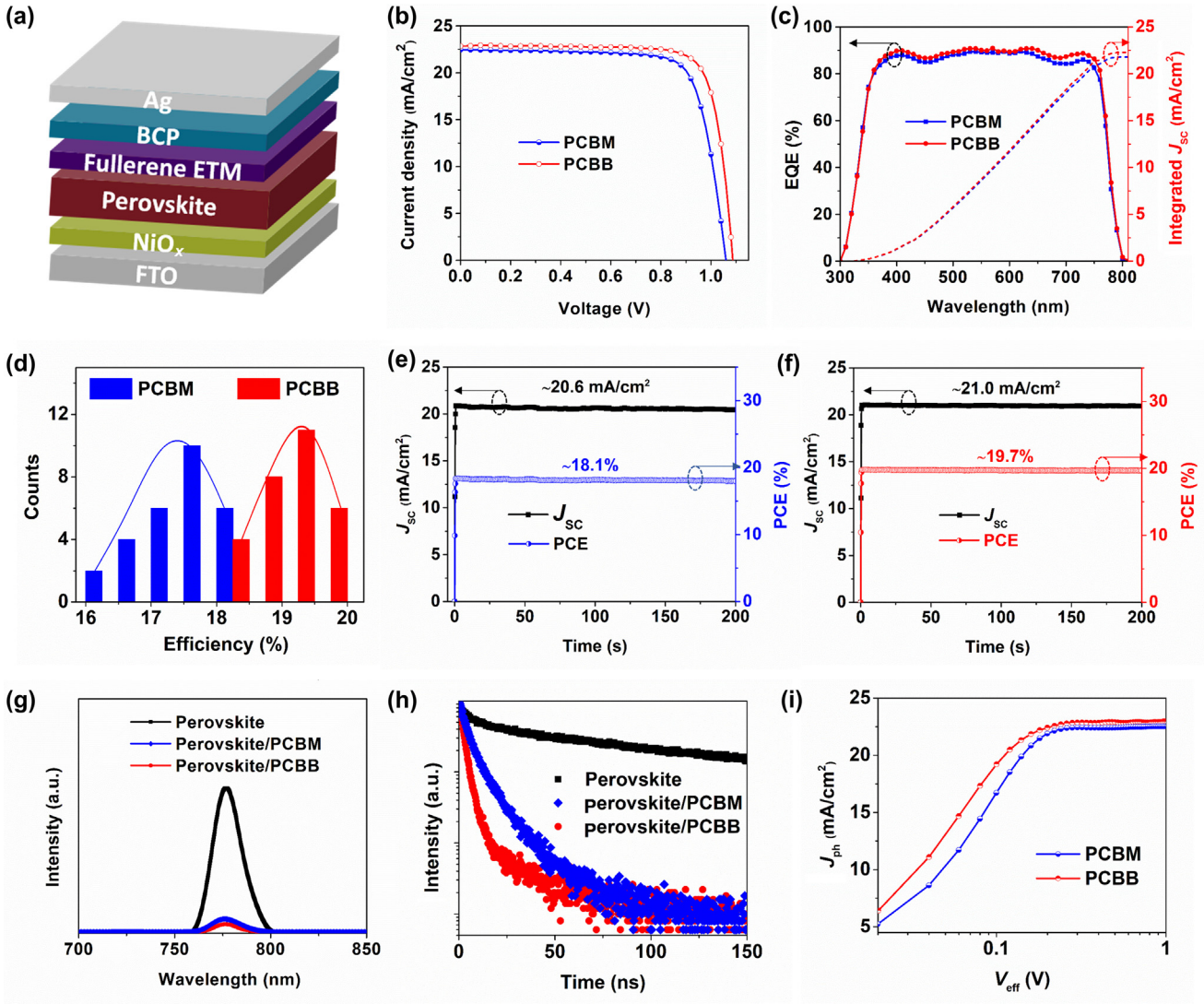

Fig. 3. Device structure and performance. (a) Device architecture of the inverted PSCs studied in this work. (b) *J-V* curves of the PCBM- and PCBB-based devices with reverse scanning direction. (c) IPCE curves (solid lines) of the devices using PCBM (blue) and PCBB (red) ETLs. The integrated photocurrents (dashed lines) calculated from the overlap integral of the EQE spectra are also shown. (d) The statistics of PCE distribution for 60 devices (30 PCBM-based devices and 30 PCBB-based devices). Steady-state photocurrent and power output at the maximum power point for (e) PCBM- and (f) PCBB-based devices at 0.88 and 0.94 V, respectively. (g) Steady-state and (h) time-resolved PL spectra of the perovskite, perovskite/PCBM, and perovskite/PCBB films. (i) Plots of J_{ph}-V_{eff} for devices with PCBM and PCBB ETLs.

extraction at the perovskite/PCBB interface [12]. The TRPL plots of the different samples were obtained as shown in Fig. 3h. We fitted the TRPL data with a biexponential equation to yield fast decay ($\tau 1$) and slow decay ($\tau 2$) processes, which originated from carrier quenching by the charge extraction layer and by radiative recombination, respectively [46,47]. As summarized in Table S4 (online), the net perovskite film exhibited a lifetime of 59.7 ns, while the PCBM- and PCBB-coated perovskite films demonstrated short photoluminescence decay times of 10.3 and 7.5 ns, respectively. These findings were consistent with the steady-state PL results. PCBB-coated perovskite films showed a much shorter lifetime of 3.87 ns ($\tau 1$) for the fast decay component than the PCBM-coated perovskite film (5.37 ns ($\tau 1$)). Thus, incorporating PCBB as ETL improved the charge extraction efficiency at the perovskite/PCBB interface and led to improved performance.

We also obtained the photocurrent density (J_{ph})–effective voltage (V_{eff}) plots under AM 1.5 G illumination for the PCBM and PCBB devices, where J_{ph} is equal to the current density at AM 1.5 G illumination minus the dark current density, and V_{eff} is equal to the voltage where J_{ph} = 0 minus the applied bias voltage [48]. As displayed in Fig. 3i, PCBB-based devices showed an enhanced J_{ph} compared with PCBM-based devices. Considering that the photogenerated charge carriers were the same for the PCBM- and PCBB-based devices, the high J_{ph} suggested that PCBB could facilitate charge extraction and reduce interfacial recombination, leading to improved device performance [49]. This result was also consistent with the tendency of the steady-state PL and TRPL measurements. In summary, the improved performance of the PCBB-based device could be reasonably interpreted as the result of efficient charge extraction at the perovskite/PCBB interface and enhanced transport owing to the high electron mobility along the compact PCBB molecule layer.

The lifetimes of the devices are closely related to the stability of the ETL, which can block the contact of moisture and oxygen with the perovskite and suppress the decomposition of the perovskite layer [50]. The stability of the ETL can also ensure the effective collection of device carriers and the high output power [51]. Thus, the intermolecular interactions and packing mode of the fullerene derivative not only affect the charge transfer properties and device efficiency but also significantly influence the long-term stability of

the device, which is a crucial parameter for the commercialization of PSCs. The change in surface morphology of the corresponding fullerene layers was investigated. As shown in Fig. 4a and d, both fullerene layers coated on the perovskite substrates were initially homogenous, with no sign of aggregation. As the illumination time increased, the atomic force microscopy (AFM) images of PCBM-based layers exhibited obvious protrusions (Fig. 4b and c), indicating the aggregation of PCBM molecules. By contrast, we did not observe any aggregation phenomena in the PCBB-based films under the same aging procedure (Fig. 4e and f). The optical microscopy images (Fig. S13 online) of the corresponding fresh and aged fullerene films exhibited the same behavior as observed by AFM. In addition, we fabricated and investigated the corresponding fullerene films on ITO substrates to avoid interference of the perovskite layer. As expected, the PCBM-based films displayed obvious aggregation after 150 h of continuous illumination with surface temperature of 55 °C, while the morphology of the PCBB-based film did not change (Fig. S14 online). These results clearly showed that the enhanced intermolecular interactions of PCBB efficiently suppressed self-aggregation and dramatically improved the stability of the films.

The photostability of the PCBM- and PCBB-based unencapsulated devices was examined using the MPP tracking method following a previous report [52]. As shown in Fig. 4g, the PCBB-based devices showed significantly improved operational stability and retained ~90% of their original efficiencies after continuous irradiation for 600 h of MPP tracking, while the PCBM-based devices rapidly dropped to 70% of their original efficiencies. Meanwhile, we explored the hydrophobicity of fullerene films through contact angle measurements. As shown in Fig. S15 (online), initial measurements for PCBM and PCBB layers had contact angles of 94° and 96°, respectively. After a short interval, significantly different

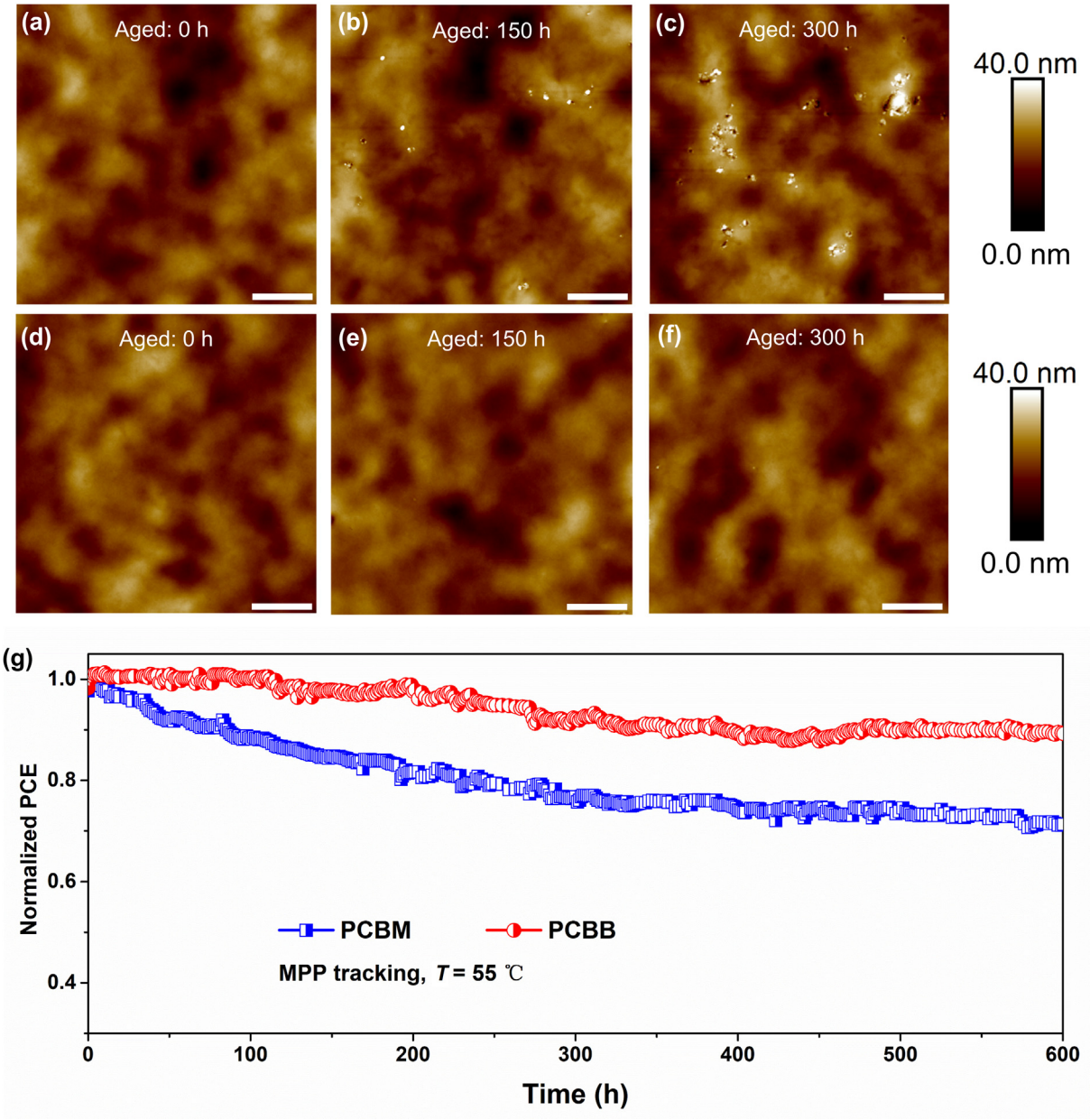

Fig. 4. Film morphology and device stability. Atomic force microscopy images of the (a–c) PCBM and (d–f) PCBB films on the perovskite substrates, which were aged under continuous illumination without cooling (surface temperature: 55 °C). The scale bar represents 1 μm. (g) The MPP tracking of the unencapsulated devices with PCBM and PCBB ETLs under continuous irradiation without cooling (surface temperature: 55 °C).

contact angles of 42° and 95° were measured for PCBM and PCBB layers, respectively. The change in contact angle of PCBM films could be attributed to the weak interaction between the PCBM molecules, which resulted in the lack of dense molecular packing and poor film stability. The evolution of contact angles indicated that the PCBB-based ETLs were more hydrophobic and more stable than the PCBM films, because of the strong intermolecular interactions in the PCBB-based films. The PCBB-based devices exhibited much higher stabilities than the PCBM-based devices under 35%–45% humidity in air at room temperature without encapsulation (Fig. S16 online). Therefore, on the basis of the abovementioned results, the intermolecular interactions of PCBB effectively promoted the high performance of PSCs.

4. Conclusion

In summary, we have demonstrated an atomic level strategy to understand and control the self-aggregation of fullerene-based ETLs for high-performance inverted PSCs. Crystal structural analyses revealed that the enhanced non-covalent intermolecular interactions of PCBB effectively facilitated electron transport between C_{60} cages, contributing to the improved electron extraction and reduced recombination in the devices. Furthermore, the densely packed PCBB molecules significantly increased the film's stability. Inverted PSC devices with PCBB as the ETL yielded an impressive efficiency of 19.84%. Device stabilities were significantly improved, retaining about 90% of the initial efficiency after 600 h under one-sun irradiation by using the MPP tracking method. This work suggests a strategy for the design of new functional fullerene derivatives to tune their intermolecular interactions in creating novel ETLs for high-performance PSCs.

Conflict of interest

The authors declare that they have no conflict of interest.

Acknowledgments

We thank financial supports from the National Natural Science Foundation of China (51902110, 51802102 and 21805101), the Scientific Research Funds of Huaqiao University (19BS105, 16BS201 and 17BS409) and Fundamental Research Funds for the Central Universities (ZQN-806, ZQN-PY607). LE also thanks the US National Science Foundation for generous support of this work under CHE-1801317. The Robert A. Welch Foundation is also gratefully acknowledged for an endowed chair to LE (AH-0033).

Author contributions

Chengbo Tian, Luis Echegoyen, and Zhanhua Wei conceived the idea and designed the experiments. Chengbo Tian conducted the experiments and drafted the manuscript. German Betancourt-Solis and Ziang Nan performed part of the synthesis and characterization of compounds. Kaikai Liu, Kebin Lin, Jianxun Lu and Liqiang Xie joined part of the experiments and analyzed the data. All authors discussed the results. Luis Echegoyen and Zhanhua Wei revised the manuscript.

Appendix A. Supplementary materials

Supplementary materials to this article can be found online at https://doi.org/10.1016/j.scib.2020.08.041.

References

[1] Kojima A, Teshima K, Shirai Y, et al. Organometal halide perovskites as visible-light sensitizers for photovoltaic cells. J Am Chem Soc 2009;131:6050–1.
[2] Jia X, Zuo C, Tao S, et al. $CsPb(I_xBr_{1-x})$ solar cells. Sci Bull 2019;64:1532–9.
[3] Noh J, Im S, Heo J, et al. Chemical management for colorful, efficient, and stable inorganic-organic hybrid nanostructured solar cells. Nano Lett 2013;13:1764–9.
[4] Stranks S, Eperon G, Grancini G, et al. Electron-hole diffusion lengths exceeding 1 micrometer in an organometal trihalide perovskite absorber. Science 2013;342:341–4.
[5] Xing G, Mathews N, Sun S, et al. Long-range balanced electron- and hole-transport lengths in organic-inorganic $CH_3NH_3PbI_3$. Science 2013;342:344–7.
[6] Nayak P, Mahesh S, Snaith H, et al. Photovoltaic solar cell technologies: analysing the state of the art. Nat Rev Mater 2019;4:269–85.
[7] Dong Q, Fang Y, Shao Y, et al. Electron-hole diffusion lengths > 175 mm in solution-grown $CH_3NH_3PbI_3$ single crystals. Science 2015;347:967–70.
[8] Rong Y, Hu Y, Mei A, et al. Challenges for commercializing perovskite solar cells. Science 2018;361:eaat8235.
[9] Zuo C, Bolink H, Han H, et al. Advances in perovskite solar cells. Adv Sci 2016;3:1500324.
[10] Zhao Y, Zhu K. Organic-inorganic hybrid lead halide perovskites for optoelectronic and electronic applications. Chem Soc Rev 2016;45:655–89.
[11] Cui D, Wang Y, Han L. China's progress of perovskite solar cells in 2019. Sci Bull 2020;65:1306–15.
[12] Fang Y, Bi C, Wang D, et al. The functions of fullerenes in hybrid perovskite solar cells. ACS Energy Lett 2017;2:782–94.
[13] Liu T, Chen K, Hu Q, et al. Inverted perovskite solar cells: progresses and perspectives. Adv Energy Mater 2016;6:1600457.
[14] Xu J, Boyd C, Yu Z, et al. Triple-halide wide–band gap perovskites with suppressed phase segregation for efficient tandems. Science 2020;367:1097–104.
[15] Chen W, Xu L, Feng X, et al. Metal acetylacetonate series in interface engineering for full low-temperature-processed, high-performance, and stable planar perovskite solar cells with conversion efficiency over 16% on 1 cm^2 scale. Adv Mater 2017;29:1603923.
[16] Park N. Research direction toward scalable, stable, and high efficiency perovskite solar cells. Adv Energy Mater 2020;10:1903106.
[17] Jeng J, Chiang Y, Lee M, et al. $CH_3NH_3PbI_3$ perovskite/fullerene planar-heterojunction hybrid solar cells. Adv Mater 2013;25:3727–32.
[18] Shao Y, Xiao Z, Bi C, et al. Origin and elimination of photocurrent hysteresis by fullerene passivation in $CH_3NH_3PbI_3$ planar heterojunction solar cells. Nat Commun 2014;5:5784.
[19] Li M, Yang Y, Wang Z, et al. Perovskite grains embraced in a soft fullerene network make highly efficient flexible solar cells with superior mechanical stability. Adv Mater 2019;31:1901519.
[20] Xing Z, Li S, Hui Y, et al. Star-like hexakis[di(ethoxycarbonyl)methano]-C60 with higher electron mobility: an unexpected electron extractor interfaced in photovoltaic perovskites. Nano Energy 2020;74:104859.
[21] Wu Y, Yang X, Chen W, et al. Perovskite solar cells with 18.21% efficiency and area over 1 cm^2 fabricated by heterojunction engineering. Nat Energy 2016;1:16148.
[22] Shao Y, Yuan Y, Huang J. Correlation of energy disorder and open-circuit voltage in hybrid perovskite solar cells. Nat Energy 2016;1:15001.
[23] Chiang C, Wu C. Bulk heterojunction perovskite–PCBM solar cells with high fill factor. Nat Photonics 2016;10:196–200.
[24] Azimi H, Ameri T, Zhang H, et al. A universal interface layer based on an amine-functionalized fullerene derivative with dual functionality for efficient solution processed organic and perovskite solar cells. Adv Energy Mater 2015;5:1401692.
[25] Tian C, Castro E, Wang T, et al. Improved performance and stability of inverted planar perovskite solar cells using fulleropyrrolidine layers. ACS Appl Mater Interfaces 2016;8:31426–32.
[26] Liu X, Lin F, Chueh C, et al. Fluoroalkyl-substituted fullerene/perovskite heterojunction for efficient and ambient stable perovskite solar cells. Nano Energy 2016;30:417–25.
[27] Li B, Zhen J, Wan Y, et al. Steering the electron transport properties of pyridine-functionalized fullerene derivatives in inverted perovskite solar cells: the nitrogen site matters. J Mater Chem A 2020;8:3872–81.
[28] Fernandez-Delgado O, Castro E, Ganivet C, et al. Variation of interfacial interactions in $PC_{61}BM$-like electron-transporting compounds for perovskite solar cells. ACS Appl Mater Interfaces 2019;11:34408–15.
[29] Gatti T, Menna E, Meneghetti M, et al. The Renaissance of fullerenes with perovskite solar cells. Nano Energy 2017;41:84–100.
[30] Pascual J, Delgado J, Tena-Zaera R. Physicochemical phenomena and application in solar cells of perovskite:fullerene films. J Phys Chem Lett 2018;9:2893–902.
[31] Zheng X, Hou Y, Bao C, et al. Managing grains and interfaces via ligand anchoring enables 22.3%-efficiency inverted perovskite solar cells. Nat Energy 2020;5:131–40.
[32] Zhang M, Chen Q, Xue R, et al. Reconfiguration of interfacial energy band structure for high-performance inverted structure perovskite solar cells. Nat Commun 2019;10:4593.
[33] Jiang X, Wang F, Wei Q, et al. Ultra-high open-circuit voltage of tin perovskite solar cells via an electron transporting layer design. Nat Commun 2020;11:1245.

[34] Wu S, Zhang J, Li Z, et al. Modulation of defects and interfaces through alkylammonium interlayer for efficient inverted perovskite solar cells. Joule 2020;4:1248–62.
[35] Christians J, Schulz P, Tinkham J, et al. Tailored interfaces of unencapsulated perovskite solar cells for >1000 hour operational stability. Nat Energy 2018;3:68–74.
[36] Yang S, Chen S, Mosconi E, et al. Stabilizing halide perovskite surfaces for solar cell operation with wide-bandgap lead oxysalts. Science 2019;365:473.
[37] Bai S, Da P, Li C, et al. Planar perovskite solar cells with long-term stability using ionic liquid additives. Nature 2019;571:245–50.
[38] Li S, Xing Z, Wu B, et al. Hybrid fullerene-based electron transport layers improving the thermal stability of perovskite solar cells. ACS Appl Mater Interfaces 2020;12:20733–40.
[39] Xiao Z, Geng X, He D, et al. Development of isomer-free fullerene bisadducts for efficient polymer solar cells. Energy Environ Sci 2016;9:2114–21.
[40] Coropceanu V, Cornil J, da Silva D, et al. Charge transport in organic semiconductors. Chem Rev 2007;107:926–52.
[41] Tian C, Castro E, Betancourt-Solis G, et al. Fullerene derivative with a branched alkyl chain exhibits enhanced charge extraction and stability in inverted planar perovskite solar cells. New J Chem 2018;42:2896–902.
[42] Rispens M, Meetsma A, Rittberger R, et al. Influence of the solvent on the crystal structure of PCBM and the efficiency of MDMO-PPV:PCBM "plastic" solar cells. Chem Commun 2003;17:2116–8.
[43] Deng L, Li X, Wang S, et al. Stereomeric effects of bis$PC_{71}BM$ on polymer solar cell performance. Sci Bull 2016;61:132–8.
[44] Mihailetchi V, Wildeman J, Blom P. Space-charge limited photocurrent. Phys Rev Lett 2005;94:126602.
[45] Sun Q, Wang H, Yang C, et al. Synthesis and electroluminescence of novel copolymers containing crown ether spacers. J Mater Chem 2003;13:800–6.
[46] Li Y, Meng L, Yang Y, et al. High-efficiency robust perovskite solar cells on ultrathin flexible substrates. Nat Commun 2016;7:10214.
[47] Liang P, Liao C, Chueh C, et al. Additive enhanced crystallization of solution-processed perovskite for highly efficient planar-heterojunction solar cells. Adv Mater 2014;26:3748–54.
[48] Chen J, Cui C, Li Y, et al. Single-junction polymer solar cells exceeding 10% power conversion efficiency. Adv Mater 2015;27:1035–41.
[49] Chen W, Zhang J, Xu G, et al. A semitransparent inorganic perovskite film for overcoming ultraviolet light instability of organic solar cells and achieving 14.03% efficiency. Adv Mater 2018;30:1800855.
[50] Wang R, Mujahid M, Duan Y, et al. A review of perovskites solar cell stability. Adv Funct Mater 2019;29:1808843.
[51] Domanski K, Correa-Baena J, Mine N, et al. Not all that glitters is gold: metal-migration-induced degradation in perovskite solar cells. ACS Nano 2016;6:6306–14.
[52] Tian C, Lin K, Lu J, et al. Interfacial bridge using a cis-fulleropyrrolidine for efficient planar perovskite solar cells with enhanced stability. Small Methods 2019;4:1900476.

Chengbo Tian received his Ph.D. degree under the supervision of Prof. Suyuan Xie from Xiamen University in 2015. After working as a postdoctoral fellow with Prof. Luis Echegoyen at University of Texas at El Paso and with Prof. Hongwei Han at Huazhong University of Science and Technology, he joined Huaqiao University as an assistant professor in 2019. His current research interest includes the coordination chemistry of fullerenes, functional fullerenes, and their photovoltaic applications.

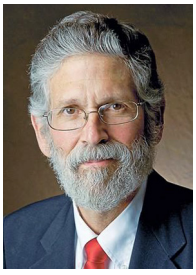

Luis Echegoyen was appointed as Chair of the Department of Chemistry at Clemson University in 2002. Later, he served as Division Director for Chemistry at the National Science Foundation for 4 years (2006–2010), and he became the Robert A. Welch Professor of Chemistry at the University of Texas at El Paso in 2010. He now serves as the president of the American Chemical Society. His research includes fullerene chemistry, electrochemistry, and supramolecular chemistry, with special emphasis on photovoltaics and endohedral fullerenes.

Zhanhua Wei is a full-time professor at the Institute of Luminescent Materials and Engineering, College of Materials Science and Engineering, Huaqiao University, China. He received his B.S. degree in 2011 from Department of Chemistry, Xiamen University, China, and his Ph.D. degree in 2015 from Prof. Shihe Yang's group, Department of Chemistry, Hong Kong University of Science and Technology, China. His current research focuses on the synthesis of perovskite materials, perovskite light-emitting diodes, perovskite solar cells, and other optoelectronic devices.